Exchange coupling constants at finite temperature

S. Mankovsky, S. Polesya, and H. Ebert
Department Chemie, Physikalische Chemie, Universität München, Butenandstr. 5-13, 81377 München, Germany

(Received 3 July 2020; accepted 29 September 2020; published 27 October 2020)

An approach to account for the effect of thermal lattice vibrations when calculating exchange coupling parameters is presented on the basis of the Korringa-Kohn-Rostoker Green function method making use of the alloy analogy model. Using several representative systems, it is shown that depending on the material the effect of thermal lattice vibrations can have a significant impact on the isotropic exchange as well as the Dzyaloshinskii-Moriya interactions (DMI). This should lead in turn to an additional contribution to the temperature dependence of the magnetic properties of solids, which cannot be neglected in the general case. As an example, we discuss such an influence on the critical temperature of various magnetic phase transitions. In particular, in the case of skyrmion hosting materials, a strong impact of lattice vibrations on the DMI is an additional source for the temperature dependent skyrmion size and stability, which should be taken into consideration. The present approach gives also access to features of magnetic properties that are associated with static atomic displacements as, for example, in random high-entropy alloys.

DOI: 10.1103/PhysRevB.102.134434

I. INTRODUCTION

The impact of finite temperatures on the various physical material properties is one of the most important issues in solid state physics that is discussed in the literature with respect to various aspects. The temperature dependence of magnetic properties is often discussed on the basis of atomistic model spin Hamiltonians, giving access to critical temperatures and allowing one to reveal the interconnection between the electronic and magnetic structure in the case of first-principles calculations of the exchange coupling parameters. However, to achieve a complete description of the thermodynamical properties of magnetic systems, that can be provided, e.g., via free energy calculations, the contributions of magnetic and lattice excitations should be taken into account together with the energy of the electronic subsystem, giving this way information on the common influence of these contributions on magnetic and structural phase transitions [1]. Corresponding DFT-based calculations by Körmann *et al.* [2] performed for bcc Fe gave an accurate description of the temperature dependent free energy and the heat capacity [2]. These authors demonstrated in addition [3] that it is important to take the magnon-phonon coupling into account when dealing with the temperature dependent modifications of the phonon modes. Indeed, theoretical methods were elaborated recently [4,5], which allow one to account for all the above mentioned contributions within coupled atomistic magnetization and lattice dynamics calculations, using the parameters calculated within a first-principles approach.

It should be stressed, however, that the interatomic exchange parameters used in such finite temperature simulations do not account for changes due to thermal lattice vibrations. However, a temperature induced modification of the electronic structure due to lattice vibrations should obviously lead in turn to corresponding changes of the exchange coupling parameters. Their dependence on the thermal lattice expansion, caused by the anharmonicity of lattice vibrations and the magnetovolume effect in magnetic systems, was considered in the literature already by different groups [6–8] together with the impact of these effects on the critical temperatures. Also the thermal lattice vibrations and spin fluctuations that may have a strong impact on the electronic structure and related physical properties can be taken into account within *ab initio* calculations using the adiabatic approximation. For that purpose, a very efficient approach—the so-called alloy analogy model—has been introduced recently [9] that allows one to account for the impact of temperature induced lattice vibrations and spin fluctuations on linear response properties, as for example the electrical and spin conductivity, the Gilbert damping, and others. In these cases, the corresponding response tensor χ_{AB} may be written as $\chi_{AB} \propto \mathrm{Tr}\langle A\,\mathrm{Im}G^{+}B\,\mathrm{Im}G^{+}\rangle_{\mathrm{T}}$, where the operators A and B represent the relevant observable and perturbation, respectively, while G^{+} stands for the retarded Green function [10]. Within the alloy analogy model lattice vibrations and spin fluctuations are treated as uncorrelated, quasistatic atomic displacements and spin tiltings, respectively, with an amplitude depending on temperature. Following the scheme used to calculate the residual resistivity of disordered alloys [10,11] by means of the single-site coherent potential approximation (CPA), the thermal average $\langle\ldots\rangle_T$ of a linear response quantity is obtained as the configurational average over a set of appropriately chosen atomic displacements and spin tiltings using the CPA alloy theory [9,12,13].

The central idea of the alloy analogy model was used already previously to account for thermal magnetic disorder when dealing with finite-temperature magnetic properties by means of first-principles calculations done on the basis of

the disordered local moment (DLM) model [14–16]. This approach was formulated at the beginning on a nonrelativistic level. Its extension to the relativistic disorder local moment (RDLM) model allowed one in particular to investigate the impact of thermal spin disorder on the magnetocrystalline anisotropy (MCA) [17–19].

So far, most calculations of the exchange parameters have been performed for ideal crystal structures assuming the *lattice temperature* $T_{\rm lat} = 0$ K. Even for this situation, already a pronounced dependence of the results on the specific atomic positions could be observed for some cases [20,21]. The significant influence of lattice vibrations on the magnon excitations of fcc Fe has been reported for example by Sabiryanov and Jaswal [22], who calculated the exchange coupling parameters accounting for corrections due to atomic displacements using a frozen-phonon scheme. A substantial change for the exchange coupling parameters in bcc Fe was also reported to be induced by a Burgers type lattice distortion which can be connected to the single N point TA_1 phonon mode [23]. Recently, a strong impact of lattice vibrations on the electronic structure and magnetic properties of materials was shown employing the disordered local moments molecular dynamics (DLM-MD) method [24,25]. This approach was also used to investigate corresponding temperature induced changes of the exchange coupling parameters, associated with thermal lattice vibrations [26]. Note that these DLM-MD calculations make use of a supercell technique to simulate thermal atomic displacements in the system. Di Gennaro *et al.* [27] have investigated the combined effects of "phononic" and "magnonic" temperatures on the spin-wave dispersion, stiffness, and Curie temperatures of Fe, Ni, and permalloy by combining first-principles methods with model Hamiltonians. Following the idea reported in Ref. [22], Di Gennaro *et al.* [27] accounted in their work for corresponding corrections to the exchange parameters associated with the thermal atomic displacements at a given temperature.

Below we present a scheme to account within the framework of the alloy analogy model for thermal lattice vibrations when calculating exchange coupling parameters. Section II represents the theoretical background for these calculations. Corresponding computational details are given in Sec. III. In Sec. IV we present results of calculations for some representative systems, which are meant to demonstrate the impact of thermal lattice vibrations on the isotropic exchange as well as on the Dzyaloshinskii-Moriya interaction parameters, J_{ij} and $\vec{D}_{ij}$, respectively. These results are complemented by calculations of the critical temperatures with and without account of thermal lattice vibrations, using a ferromagnetic or DLM, respectively, reference state.

II. THEORETICAL BACKGROUND

In the following the temperature dependence of the parameters of the extended Heisenberg Hamiltonian

$$H_{ex} = -\sum_{ij} J_{ij}(\hat{e}_i \cdot \hat{e}_j) - \sum_{ij} \vec{D}_{ij}[\hat{e}_i \times \hat{e}_j] \tag{1}$$

will be considered. Here J_{ij} is the isotropic exchange coupling parameter connected with the spin moments on sites i and j pointing along the directions $\hat{e}_i$ and $\hat{e}_j$, respectively, while $\vec{D}_{ij}$ represents the Dzyaloshinskii-Moriya (DM) interaction. We will focus first of all on the properties of the isotropic exchange parameters J_{ij}, which are given by the average over the diagonal elements of the exchange coupling tensor [28]. Making use of relativistic multiple-scattering formalism the elements of this tensor can be written for $T = 0$ K as [29]

$$J_{ij}^{\alpha_i\alpha_j} = -\frac{1}{2\pi}\mathrm{Im}\int dE\ \mathrm{Tr}\,\Delta\underline{V}^{\alpha_i}(E)\underline{\tau}^{ij}(E)\Delta\underline{V}^{\alpha_j}(E)\underline{\tau}^{ji}(E). \tag{2}$$

Here $\underline{\tau}^{ij}$ is the so-called scattering path operator connecting sites i and j with the underline indicating matrices in the $\Lambda = (\kappa, \mu)$ representation [30]. The corresponding on-site coupling for site i is represented by the matrix [29]

$$\Delta V_{\Lambda\Lambda'}^{\alpha_i} = \int d^3r\, Z_{\Lambda}^{\times}(\vec{r}, E)\beta\sigma_\alpha B(r) Z_{\Lambda'}(\vec{r}, E), \tag{3}$$

where β is one of the standard Dirac matrices, σ_α is a (4×4)-Pauli matrix [30] and $B(r) = |\vec{B}(r)|$, where $\vec{B}(r) = B(r)(0, 0, 1)$ is the spin-dependent part of the exchange-correlation potential set up within local spin-density theory [29]. Finally, the wave functions $Z_\Lambda(\vec{r})$ are solutions to the Dirac equation normalized according to the relativistic multiple-scattering formalism [31].

To apply the expression in Eq. (2) for the case of lattice vibrations at finite temperatures, we use again the alloy analogy model based on the adiabatic approximation [12,13]. This implies that a discrete set of N_v displacement vectors $\Delta\vec{R}_v^q(T)$ with probability x_v^q $(v = 1, \ldots, N_v)$ is constructed for each basis atom q within the crystallographic unit cell. The vectors $\Delta\vec{R}_v^q(T)$ are connected with the temperature dependent root mean square (rms) displacement $(\langle u^2\rangle_T)^{1/2}$ according to the relation

$$\sum_{v=1}^{N_v} x_v^q \left|\Delta\vec{R}_v^q(T)\right|^2 = \left\langle u_q^2\right\rangle_T. \tag{4}$$

For the applications presented below, we follow the idea used within previous temperature dependent linear-response calculations [9], where the temperature dependent rms displacement is estimated using Debye's theory. This approach provides a simple connection between $\langle u_q^2\rangle_T$ and the *lattice temperature* via the expression [32–34]

$$\langle u^2\rangle_T = \frac{9\hbar^2}{M k_{\rm B}\Theta_D}\left[\frac{\Phi(\Theta_D/T)}{\Theta_D/T} + \frac{1}{4}\right], \tag{5}$$

with $\Phi(\Theta_D/T)$ the Debye function and Θ_D the Debye temperature. Due to the restrictions of the Debye model, the same rms displacement is applied to all atoms in the case of complex systems. In this case, Eq. (5) is evaluated using the average mass M of the atoms in the system and the Debye temperature Θ_D taken from experiment. As the estimation of the rms displacements corresponding to a given *lattice temperature* may be not accurate enough, we give in all figures both the *lattice temperature* as well as the amplitude of the rms displacements. Following Ref. [9], we ignore here the zero temperature term 1/4 and assume a frozen potential for the displaced atoms. The probability x_v for a specific displacement v is chosen as $1/N_v$, i.e., equal weights are used for all displacements.

To simplify notation we restrict the expressions below to systems with one atom per unit cell. The index q numbering sites in the unit cell can therefore be dropped, while the index n numbers the lattice sites.

Each displacement vector $\Delta\vec{R}_v(T)$ determines a corresponding U-matrix $\underline{U}_v$ that describes for all matrices in the Λ representation the coordinate transformation from a shifted atom position to the original equilibrium position. This allows one in particular to connect the single-site t-matrix $\underline{t}_v$ for a shifted atom to the common global frame of reference used by the multiple scattering calculations. Within the alloy analogy model, each member in the set of N_v displacement vectors $\Delta\vec{R}_v(T)$ can now be seen as a pseudocomponent of a multicomponent pseudoalloy. As for a substitutional alloy, the site diagonal configurational average can this way be determined by solving the multicomponent CPA equations referring to the global frame of reference:

$$\underline{\tau}_{\rm CPA} = \sum_{v=1}^{N_v} x_v \underline{\tau}_v, \tag{6}$$

$$\underline{\tau}_v = [(\underline{t}_v)^{-1} - (\underline{t}_{\rm CPA})^{-1} + (\underline{\tau}_{\rm CPA})^{-1}]^{-1}, \tag{7}$$

$$\underline{\tau}_{\rm CPA} = \frac{1}{\Omega_{\rm BZ}} \int_{\Omega_{\rm BZ}} d^3k [(\underline{t}_{\rm CPA})^{-1} - \underline{G}(\vec{k}, E)]^{-1}, \tag{8}$$

where the CPA medium is described by a corresponding CPA single-site t-matrix $\underline{t}_{\rm CPA}$ and scattering path operator $\underline{\tau}_{\rm CPA}$. The first of these equations expresses the requirement for the mean-field CPA medium that embedding of a component v into the medium should not lead in the average to an additional scattering, with Eq. (7) giving the corresponding scattering path operator $\underline{\tau}_v$ for the embedded component v. Finally, Eq. (8) gives $\underline{\tau}_{\rm CPA}$ by a Brillouin zone integral in terms of $\underline{t}_{\rm CPA}$ and the so-called Korringa-Kohn-Rostoker (KKR) structure constants $\underline{G}(\vec{k}, E)$ [35].

Assuming—in line with the adiabatic approximation—a frozen potential for the displaced atoms and neglecting correlations between the atomic displacements, Eqs. (6) to (8) allow one to evaluate the necessary thermal configurational averaging when dealing with Eq. (2) for finite temperatures. This way one gets for the temperature dependent exchange coupling constants

$$\bar{J}_{ij}^{\alpha_i\alpha_j} = -\frac{1}{2\pi} {\rm Im} \int dE \, {\rm Tr} \langle \Delta\underline{V}^{\alpha_i} \underline{\tau}^{ij} \Delta\underline{V}^{\alpha_j} \underline{\tau}^{ji} \rangle_c, \tag{9}$$

where $\langle \ldots \rangle_{\rm c}$ represents the configurational average with respect to the set of displacements. In all calculations we have used a set of $N_v = 14$ displacements as increasing N_v led only to minor changes to the final results. Note also that within the present work the temperature dependent changes of the occupation numbers for the electronic states are not taken into account. As discussed in the context of the electrical conductivity dealing with thermal lattice vibrations, a configurational average as occurring in Eq. (9) leads to the so-called vertex corrections [10,11]. As the expression in Eq. (9) refers explicitly to a specific pair of sites, these have been ignored here; i.e., the configuration average has been simplified to $\langle \Delta\underline{V}^{\alpha}\ \underline{\tau}^{ij} \rangle_{\rm c} \langle \Delta\underline{V}^{\beta}\ \underline{\tau}^{ji} \rangle_{\rm c}$.

III. COMPUTATIONAL DETAILS

The results presented below are based on self-consistent first-principles electronic structure calculations performed using the spin-polarized relativistic Korringa-Kohn-Rostoker Green function (SPR-KKR-GF) method [35,36], using the atomic sphere approximation (ASA). The local spin density approximation (LSDA) to spin density functional theory (SDFT) has been used with a parametrization for the exchange and correlation potential as given by Vosko *et al.* [37]. For the angular momentum expansion of the Green function the angular momentum cutoff $l_{\rm max} = 3$ was used. Within the present work, the following systems have been considered: bcc Fe ($a = 5.41$ a.u.; $\Theta_D = 420$ K), fcc Ni ($a = 6.65$ a.u.; $\Theta_D = 375$ K), ferromagnetic ($a = 5.66$ a.u.), and antiferromagnetic ($a = 5.63$ a.u.) B2 FeRh with $\Theta_D = 390$ K for both phases, 1 ML Fe on the (111) surface of Pt ($a = 7.40$ a.u. for fcc Pt; $\Theta_D = 280$ K), and 1 ML Fe on the (111) surface of Au ($a = 7.68$ a.u. for fcc Au; $\Theta_D = 230$ K) with the corresponding structure parameters given in atomic units, i.e., as multiples of the Bohr radius, in parentheses. The calculations for 1 ML Fe/Pt(111) and 1 ML Fe/Au(111) have been performed using a supercell geometry with a (1 ML Fe/3 ML Pt(Au)/5 ML ES) supercell (where ES stands for empty sphere), with Fe occupying ideal fcc positions, i.e., without optimization of the interlayer distance. A k-mesh with $25 \times 25 \times 25$ grid points was used for the integration over the BZ of the three-dimensional bulk systems and with $46 \times 46 \times 5$ grid points for 1 ML Fe on the (111) surface of Pt or Au, respectively. For the calculations of the exchange parameters as a function of the occupation the corresponding energy integration has been performed using an energy mesh with 200 energies having a constant imaginary part of 1 meV.

IV. RESULTS AND DISCUSSION

A. bcc Fe

As it is mentioned above, one may expect that the modification of the electronic structure due to thermal lattice vibrations will not only influence transport and other response properties, but also the exchange coupling parameters. That this is indeed the case is demonstrated in the following for the elemental ferromagnets bcc Fe and fcc Ni, B2 bulk FeRh, as well as for a Fe monolayer on Pt(111) as representative examples.

The isotropic exchange coupling parameters J_{ij} calculated for the FM reference state of bcc Fe are plotted in Fig. 1 (a) for different amplitudes of thermal lattice vibrations related to a corresponding *lattice temperature* $T_{\rm lat}$ according to the Debye model. As one can see, there are indeed pronounced modifications of the exchange coupling parameters due to the lattice vibrations that depend strongly on the considered pair of sites. By far the most significant changes are found for the nearest-neighbor interaction parameters that decrease strongly with an increase of the amplitude of the thermal displacements or the *lattice temperature*, respectively. This in turn should have a corresponding impact on the Curie temperature $T_{\rm C}$. Within the mean-field approximation (MFA), $T_{\rm C}$ is essentially given by a sum $\sum_j J_{ij}$ over the coupling parameters allowing therefore in a simple way to monitor the dependence of $T_{\rm C}$

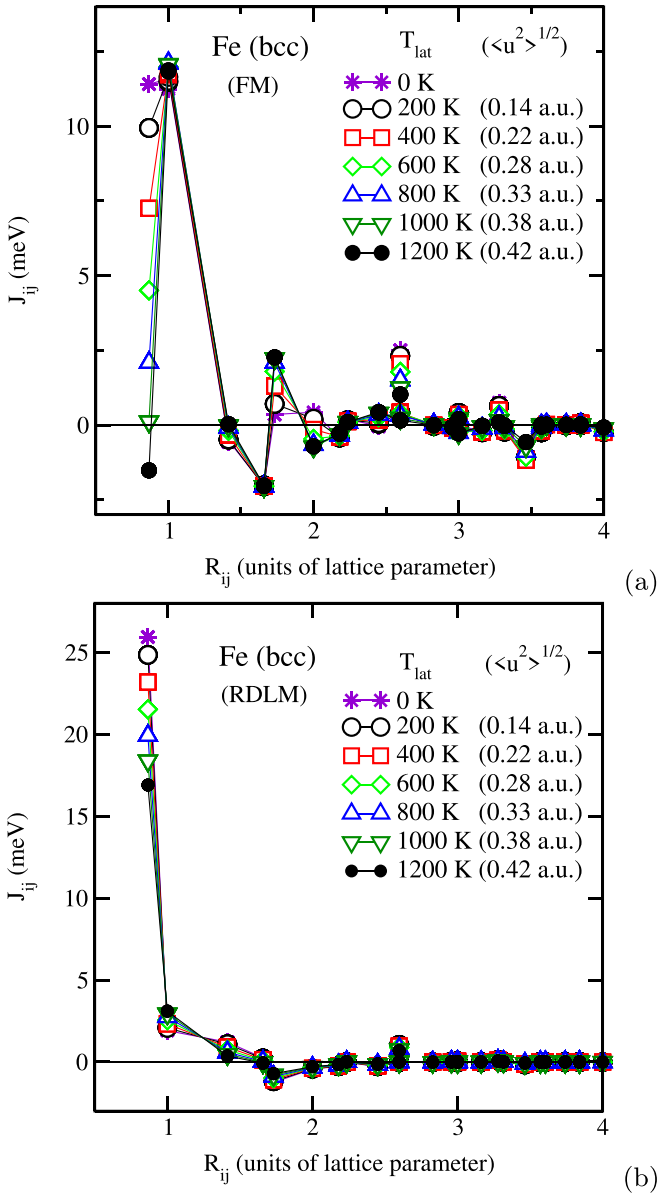

FIG. 1. Isotropic exchange coupling parameters J_{ij} for bcc Fe calculated for the FM (a) and DLM (b) reference states. The results are represented for different amplitudes of the thermal lattice vibrations given in terms of the rms displacement $(\langle u^2\rangle_T)^{1/2}$ and corresponding *lattice temperature* $T_{\rm lat}$.

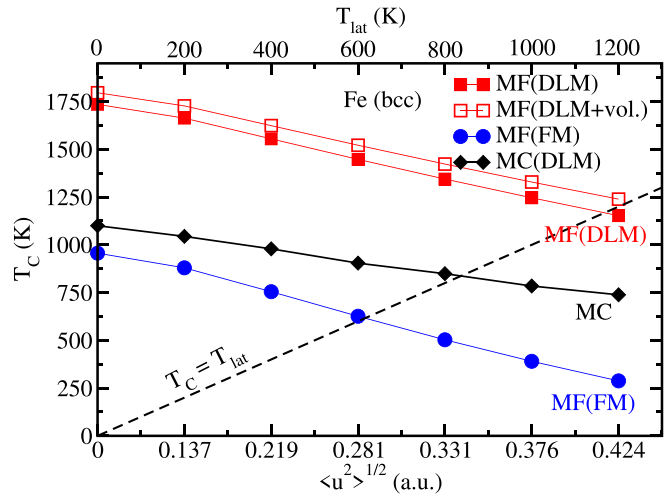

FIG. 2. Theoretical Curie temperature $T_{\rm C}$ for bcc Fe plotted as a function of the amplitudes of thermal lattice vibrations $(\langle u^2\rangle_T)^{1/2}$ calculated for the FM (circles) and DLM reference states either using the MFA (squares) or MC simulations (diamonds) together with the relation between the *lattice temperature* $T_{\rm lat}$ and $(\langle u^2\rangle_T)^{1/2}$. Open squares represent the results on DLM-based mean-field $T_{\rm C}$ calculated for lattice parameter corresponding to experimental Curie temperature.

on the effective *lattice temperature* $T_{\rm lat}$ or, equivalently, on the temperature dependent rms displacement $(\langle u^2\rangle_T)^{1/2}$. Figure 2 (circles) shows corresponding results for $T_{\rm C}$ as a function of $(\langle u^2\rangle_T)^{1/2}$ obtained by summing J_{ij} within a sphere with radius $R_{\rm max} = 5a$, with a being the lattice parameter.

Keeping in mind that the mean field approximation (MFA) normally overestimates the critical temperature when compared to results obtained from Monte Carlo (MC) simulations or RPA (random phase approximation) based calculations, one notes that the MFA result for $T_{\rm C}$ of bcc Fe, evaluated without accounting for the lattice vibrations, is rather close to the experimental value, $T_{\rm C}^{\rm exp} = 1043$ K. However, a finite amplitude of the lattice vibrations leads to a significant monotonous decrease of $T_{\rm C}^{\rm MF}$ with $(\langle u^2\rangle_T)^{1/2}$ implying a corresponding deviation from experiment. As mentioned above, more reliable results for the Curie temperature can be obtained on the basis of the exchange coupling parameters calculated for the PM reference state described here within the disordered local moment (DLM) approximation. Using the nonrelativistic version of this model, magnetic disorder in the PM state is accounted for by averaging over all possible directions of the spin moments. Equivalent to this is to consider a pseudoalloy $Fe_{0.5}^{\rm up}Fe_{0.5}^{\rm down}$ of Fe atoms with opposite spin moments oriented up and down, respectively. This leads to a significant modification of the electronic structure at high temperature when compared to the case when only lattice vibrations are taken into account. This is demonstrated by Fig. 3, which shows for bcc Fe at the *lattice temperature* $T_{lat} = 1200$ K the spin-projected DOS in the global frame of reference, calculated accounting for lattice vibrations only (FM reference state) as well as with spin fluctuations included (DLM reference state). Treating the magnetically disordered state within the DLM approach implies a random orientation of the atomic spin magnetic moments leading to the same spin-up and spin-down DOS in the global frame in spite of the exchange split electronic states with their quantization axis oriented along the atomic spin magnetic moment. These results are compared in Fig. 3 with the DOS calculated for $T_{lat} = 0$ K. The significant difference of the electronic structure for the magnetically disordered state compared to that for the FM state leads to a corresponding difference for the exchange coupling parameters. Figure 1(b) gives the resulting exchange coupling parameters for the DLM reference state of Fe. As a consequence, the corresponding MFA Curie temperature ($\approx$1700 K) exceeds the value obtained for the FM reference state in an appreciable way when thermal lattice vibrations

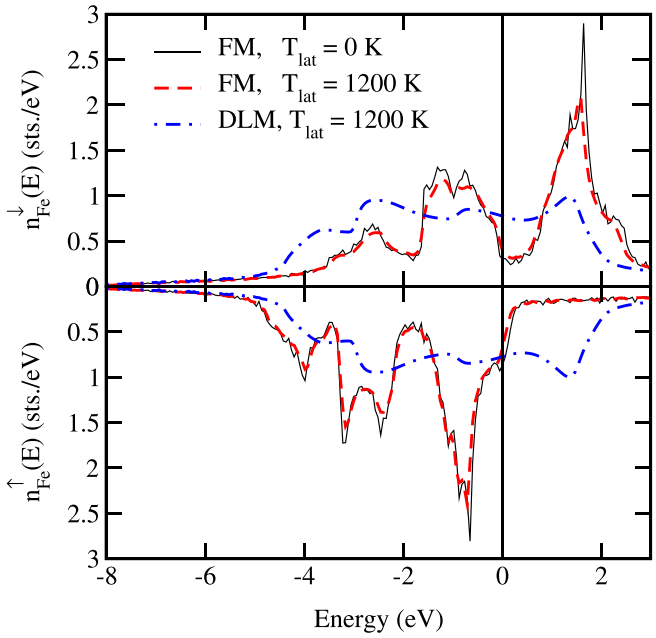

FIG. 3. Spin-projected DOS for bcc Fe, calculated accounting for thermal lattice vibrations only (dashed line, FM reference state) and thermal lattice vibrations + spin fluctuations (dashed-dotted line, DLM reference state) for $T_{\rm lat} = 1200$ K. Solid line represents the ground state DOS calculated for the FM reference state.

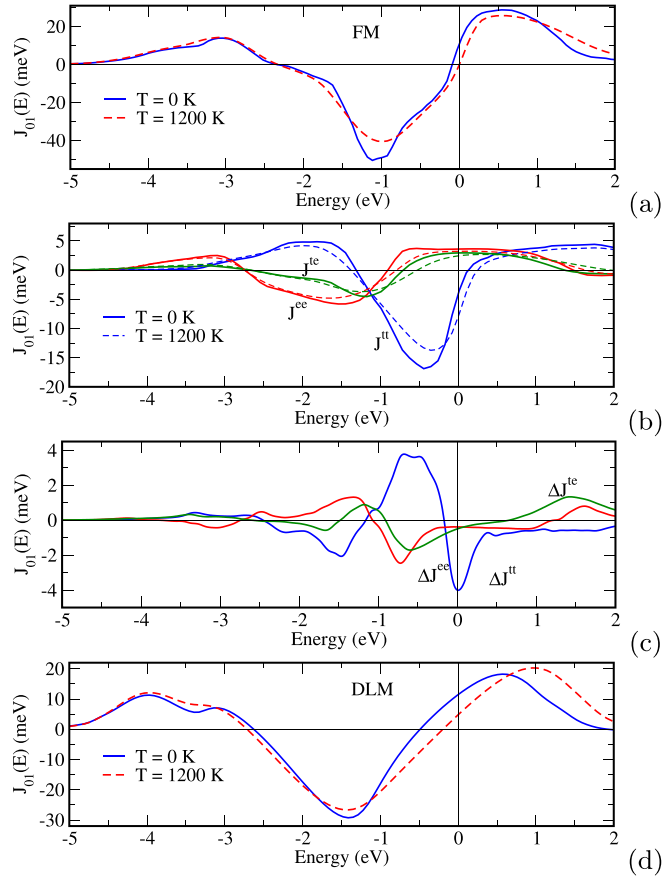

FIG. 4. Occupation dependence of the exchange coupling parameter J_{01} of bcc Fe for the FM (a) and the DLM (c) reference states. Dashed line represents results for the *lattice temperature* $T_{\rm lat} =$ 1200 K. Panel (b) represents the orbital-resolved parameters for the FM reference state, $\tilde{J}^{tt}_{01}$, $\tilde{J}^{ee}_{01}$, and $\tilde{J}^{te}_{01}$, respectively, while (c) gives their changes due to thermal lattice vibrations when increasing $T_{\rm lat}$ from 0 to 1200 K.

are ignored. This observation was already reported in the literature before (see, e.g., Ref. [38]). A finite amplitude of the thermal atomic displacements leads again to a lower MFA-based Curie temperature, as it is shown in Fig. 2 (squares), reaching the value $T_{\rm C}^{\rm MF} \approx 1200$ K when requiring that the Curie temperature and *lattice temperature* coincide. In order to compare the impact of thermal lattice vibrations on the exchange interactions with the impact of a thermal lattice expansion, the DLM-based calculations have been performed also for bcc Fe with the lattice parameter $a = 5.48$ a.u. as determined for the Curie temperature [39]. The mean-field results for T_C obtained in this case show only a rather small increase when compared to the case without account of lattice expansion (open squares in Fig. 2). This implies a dominating influence on J_{ij} for thermal lattice vibrations when compared to the impact of the thermal lattice expansion.

Figure 2 gives also results for the Curie temperature obtained by MC simulations considering 15 atomic shells around each atom using DLM-based exchange parameters (diamonds). In this case, the Curie temperature $T_{\rm C}^{\rm MC}$, calculated for an unperturbed lattice, slightly overestimates the experimental value. When the amplitude of thermal lattice vibrations increases, $T_{\rm C}^{\rm MC}$ also goes down and coincides with the *lattice temperature* $T_{\rm lat}$ at around 1000 K, underestimating slightly the experimental Curie temperature this way. This small deviation might among others be ascribed to the approximate treatment of lattice vibrations when calculating J_{ij} that in particular neglects correlations in the thermal motion of the atoms.

To get more insight concerning the temperature dependence of the exchange coupling parameters, Fig. 4(a) shows the nearest-neighbor parameter J_{01} for FM bcc Fe for two different temperatures as a function of the upper limit of the energy integration in Eq. (2) (with $E = 0$ eV the true Fermi energy) reflecting its dependence on the occupation. The solid and dashed lines represent results obtained without and with lattice vibrations, respectively, accounted for. One can see that depending on the occupation of the valence band the lattice vibrations can result either in a decrease or increase of the exchange parameter. Following the idea reported by Wang *et al.* [8] and later by Kvashnin *et al.* [40] and Ruban and Peil [26], one can further decompose J_{ij} into its orbital contributions. For the orbitals grouped according to the representations of the cubic point group, t_{2g} and e_g, the exchange parameter can be decomposed according to the expression $J_{ij} = J_{ij}^{t_{2g}-t_{2g}} + J_{ij}^{e_g-e_g} + J_{ij}^{t_{2g}-e_g}$ allowing one to monitor the dependence of the individual orbital contributions to J_{ij} on the lattice vibrations [26]. In Fig. 4(b) representative results are shown for the contributions of the $l = 2, m = \pm 1$ (t_{2g}) and $l = 2, m = 0$ orbitals (e_g) to the nearest neighbor interaction parameter J_{01}, with the corresponding representations given in parentheses. To distinguish these data from those connected with the complete set of the cubic point group representations, t_{2g} and e_g, we use the symbol $\tilde{J}$ instead of J.

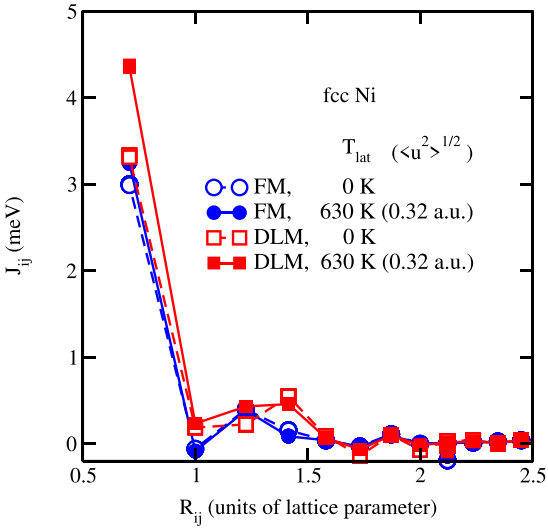

FIG. 5. Exchange coupling parameters J_{ij} calculated for Ni for the FM and DLM reference state without lattice vibrations and accounting for lattice vibrations corresponding to $T_{\text{lat}} = 630$ K.

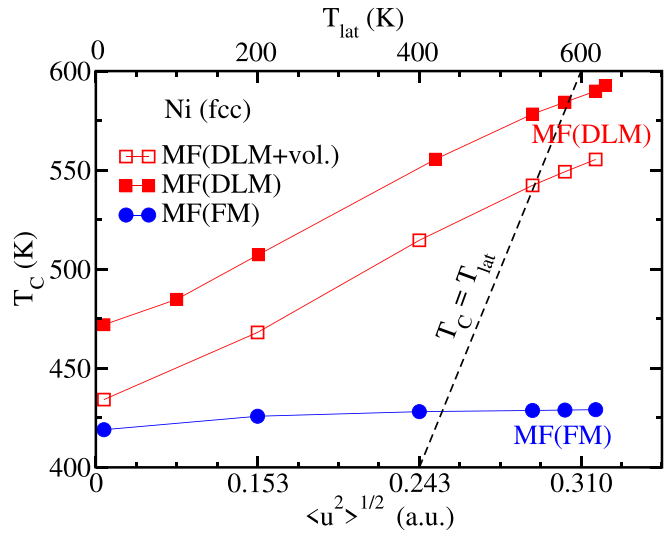

FIG. 6. MF Curie temperature calculated for fcc Ni for the FM (circles) and DLM (squares) reference states, plotted as a function of the amplitudes of thermal lattice vibrations given in terms of *lattice temperature*. Open squares represent the results on DLM-based mean-field T_{C} calculated for lattice parameter corresponding to experimental Curie temperature.

For calculations done without lattice vibrations ($T_{\text{lat}} = 0$ K), this decomposition reveals an antiferromagnetic character for the $\tilde{J}_{01}^{tt}$ parameter in contrast to the ferromagnetic character of $\tilde{J}_{01}^{ee}$ and $\tilde{J}_{01}^{te}$. This finding is in full agreement with previous work [26,40]. The change of the orbital resolved coupling parameters $\tilde{J}_{01}^{\gamma\gamma'}$ [$\gamma(\gamma') = e \equiv e_g,\ t \equiv t_{2g}$] when going from 0 to 1200 K is shown in Fig. 4(c). Obviously, the most pronounced changes are found for the contribution $\tilde{J}_{01}^{tt}$. The observed changes are primarily ascribed to the broadening of the electronic states due to the thermal lattice vibrations, leading either to an increase or decrease of $\tilde{J}_{01}^{\gamma\gamma'}$ or J_{01}, respectively, depending on the occupation of the energy band. Finally, Fig. 4(d) represents results obtained for the DLM reference state. The electronic states in this case are broadened in addition due to the thermally induced magnetic disorder in the system. Including thermal lattice vibrations in addition with $T_{\text{lat}} = 1200$ K leads for the J_{01} parameter to changes with respect to $T_{\text{lat}} = 0$ K, comparable to those found for the ferromagnetic reference state [see Fig. 4(a)].

B. fcc Ni

The isotropic exchange coupling parameters J_{ij} calculated for fcc Ni are shown in Fig. 5. For this material the lattice vibrations lead to a tiny modification of the exchange parameters calculated for the FM reference state for $T_{\text{lat}} = 0$ (open circles) and 630 K (closed circles) shown in Fig. 5. The mean-field Curie temperature evaluated with these parameters increases from $T_{\text{C}}^{\text{MF}} \approx 420$ K obtained with the parameters for the unperturbed ground state ($T_{\text{lat}} = 0$ K) to $T_{\text{C}}^{\text{MF}} \approx 430$ K for the state with an amplitude of lattice vibrations corresponding to $T_{\text{lat}} = 630$ K. The well known itinerant-electron character of magnetism in Ni leads—in contrast to Fe—for the PM state above the Curie temperature to a very small or vanishing magnetic moment (see, e.g., Ref. [41] and references therein). This prevents one from performing standard self-consistent DLM calculations as these also lead to a zero local magnetic moment for the paramagnetic DLM state. For that reason, Ruban *et al.* suggested using a constrained local exchange field when dealing with the magnetic properties of Ni. As the subtle temperature dependent magnetism of Ni is not the central issue of the present work, we investigated the simultaneous impact of lattice vibrations and magnetic disorder on the J_{ij} parameters by performing the DLM-like calculations with the spin moment constrained by using a frozen potential [9,12,13]. The resulting exchange coupling parameters calculated for the DLM reference state without account for lattice vibrations are given in Fig. 5 by open squares, while closed squares represent data for the *lattice temperature* $T_{\text{lat}} = 630$ K. As one notes, the first-neighbor exchange parameters significantly increase with the temperature increase as can be seen in Fig. 5. The corresponding MFA Curie temperature shown in Fig. 6 by squares increases from ~470 K for $T_{\text{lat}} = 0$ K to ~600 K for $T_{\text{lat}} = 630$ K. However, one should keep in mind that the MFA results lead usually to an overestimation of the Curie temperature. On the other hand, performing instead MC simulations based on the DLM derived exchange parameters calculated for $T_{\text{lat}} = 630$ K leads to a Curie temperature $T_{\text{C}} = 430$ K that is far below the experimental value.

The mean-field Curie temperature was calculated also using the DLM-based exchange coupling parameters, taking into account the thermal lattice expansion and using the lattice parameter measured at the Curie temperature [42]. The corresponding results are given in Fig. 6 by open squares, showing in contrast to bcc Fe a decrease of T_C. Note, however, that the impact of the lattice expansion on the Curie temperature is found to be smaller than the impact of thermal lattice vibrations, similar to the case of bcc Fe.

The occupation dependence of the exchange coupling parameter J_{01} of Ni calculated for the FM reference state is

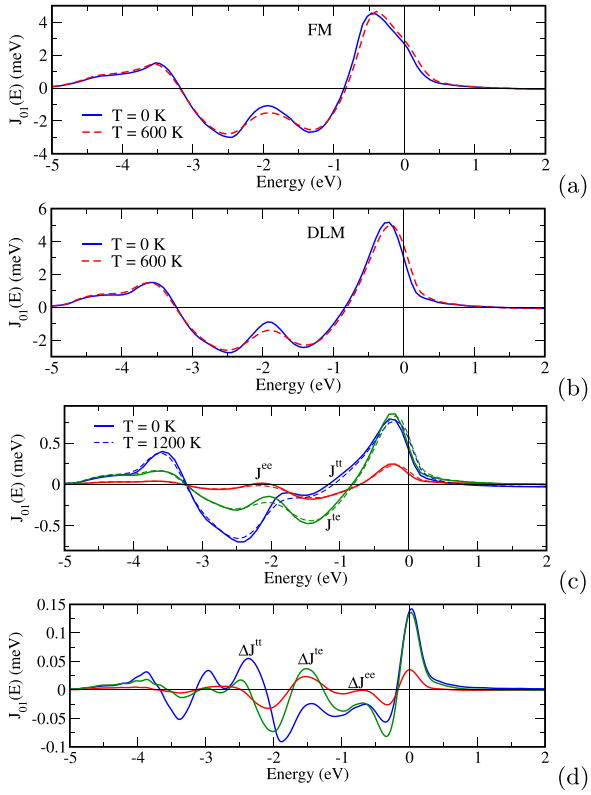

FIG. 7. Occupation dependent exchange coupling parameter J_{01} for fcc Ni for the FM (a) and the DLM (b) reference states. Panel (c) represents the orbital-resolved parameters for the DLM reference state, $\tilde{J}^{tt}_{01}$, $\tilde{J}^{ee}_{01}$, and $\tilde{J}^{te}_{01}$ and (d) their changes due to thermal lattice vibrations.

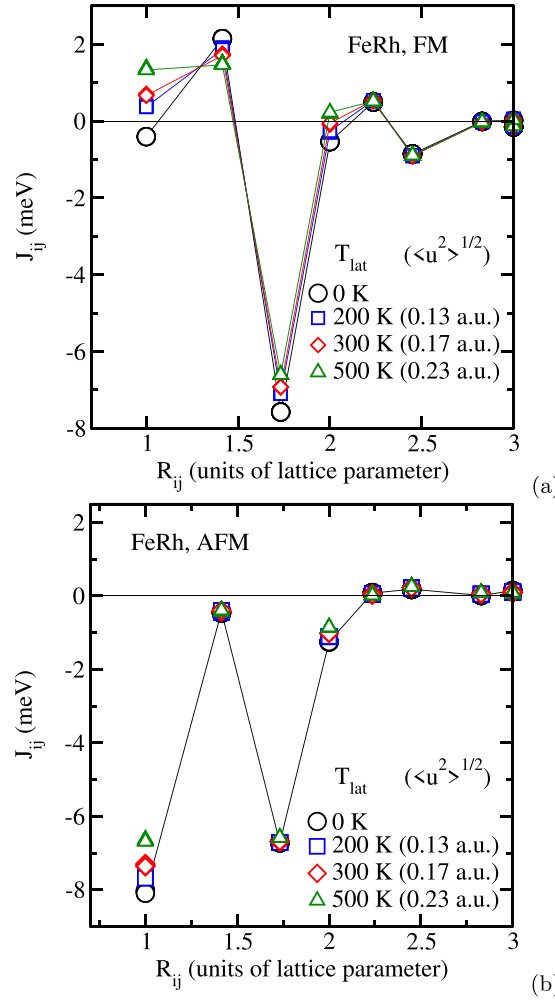

FIG. 8. Interatomic Fe-Fe exchange coupling parameters corresponding to various temperatures, calculated for FeRh with the FM (a) and AFM (b) structures. The temperature dependence is only due to the thermal lattice vibrations. The mean-square displacements corresponding to the considered temperatures are as follows: 0.13 a.u. (200 K), 0.17 a.u. (300 K), and 0.23 a.u. (500 K).

shown in Fig. 7(a) for the two *lattice temperatures* $T_{\rm lat} = 0$ and 630 K. As to be expected from Fig. 5 a relatively weak impact of thermal lattice vibrations is found in this case. This can partially be attributed to the rather low critical temperature, i.e., temperature regime to be considered, for which the mean-square displacements of the atoms are still too small to lead to significant changes in the electronic structure. In line with this, the temperature dependence of the parameter for the DLM reference state shown in Fig. 7(b) is found to be very similar to that for the FM state. The orbital decomposition of the data for the DLM reference state that is given in Fig. 7(c) shows that all components $\tilde{J}^{tt}_{01}$, $\tilde{J}^{ee}_{01}$, and $\tilde{J}^{te}_{01}$ are positive for the occupation corresponding to the true Fermi energy of fcc Ni and that for Ni the most pronounced impact of lattice vibrations occurs for the $\tilde{J}^{tt}_{01}$ and $\tilde{J}^{te}_{01}$ contributions.

C. FeRh

As an example for a compound, the well known B2 FeRh system that exhibits a temperature induced AFM to FM transition is considered in the following. According to first-principles calculations [43], the metamagnetic transition can be seen as a result of the competition of Fe-Fe exchange interactions including indirect Fe-Rh-Fe interactions, which depend on the magnetic configuration. However, a possible influence of lattice vibrations on the finite temperature magnetic properties of FeRh has not been discussed so far. Within the present work, calculations have been performed for the FM and AFM configurations separately considering several values of *lattice temperatures*. The corresponding results are given in Fig. 8 for the FM (a) and AFM (b) states. One can see in both cases that the increase of the amplitude of the thermal lattice vibrations results in an increase of the interatomic FM exchange and a decrease of the AFM exchange interactions. According to the discussions in Ref. [43], these changes of the Fe-Fe exchange interactions should lead in the AFM phase to an increase of the amplitude of the thermally induced spin fluctuations and in turn to an increase of the amplitude of the fluctuations of the induced Rh magnetic moments that are responsible for the stabilization of the FM state [43]. Corresponding MC simulations have been performed following the approach reported in Ref. [43] using the Fe-Fe exchange parameters calculated accounting for thermal lattice vibrations corresponding to the *lattice temperature* $T_{\rm lat} = 300$ K. The calculations lead a decrease of the critical temperature for the AFM-FM metamagnetic phase transition by about

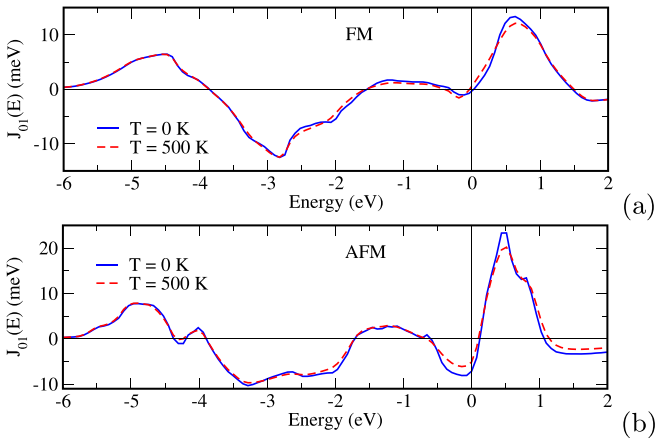

FIG. 9. Occupation dependent Fe-Fe exchange coupling parameter J_{01} for FeRh using the FM (a) and the AFM (b) structure as reference states. The results are presented for two values of the *lattice temperature* T_{lat}.

40 K. It should be noted that in these simulations the Fe-Rh exchange interactions have been taken the same as those used in Ref. [43], i.e., calculated for $T_{\text{lat}} = 0$ K without including the impact of lattice vibrations.

The occupation dependence of the Fe-Fe exchange coupling parameter J_{01} of FeRh is shown in Fig. 9 for the FM as well as the AFM reference states. One can see that the impact of lattice vibrations on J_{ij} is rather small over all occupation numbers or energies, respectively, and is close to its maximum value for the proper occupation number at the Fermi level, i.e., at $E = 0$ eV.

D. Two-dimensional systems: 1 ML Fe on Pt(111) and Au(111)

Finally, as an example for two-dimensional (2D) systems, we present results for 1 ML Fe on a Pt(111) and a Au(111) substrate, composed of three atomic layers, respectively. These model systems are considered here only as illustrative examples. Because of the lack of inversion symmetry the Dzyaloshinskii-Moriya interaction (DMI) is finite in these systems, allowing one to discuss the impact of lattice vibrations not only on the isotropic exchange interactions but also on the DMI. It should be noted here that a temperature dependency of the DMI has been observed in experiment by several groups [44,45], while so far no corresponding theoretical discussion can be found in the literature to our knowledge.

In contrast to the bulk materials discussed above, the 2D systems considered here are strongly anisotropic. This implies that the approximations used to characterize thermal lattice vibrations, i.e., in particular assuming isotropic displacements of the surface atoms, are less justified. This problem, however, can be removed by accounting for the directional anisotropy of the displacements with the necessary input taken from additional phonon calculations, as it was reported recently [46]. Another simplification is the use of the Debye temperature of corresponding bulk materials of the overlayer and substrate, as experimental data for the specific surface layer system are not available. It should be noted also that, in spite of the lack of translation symmetry in one direction, the half-infinite surface

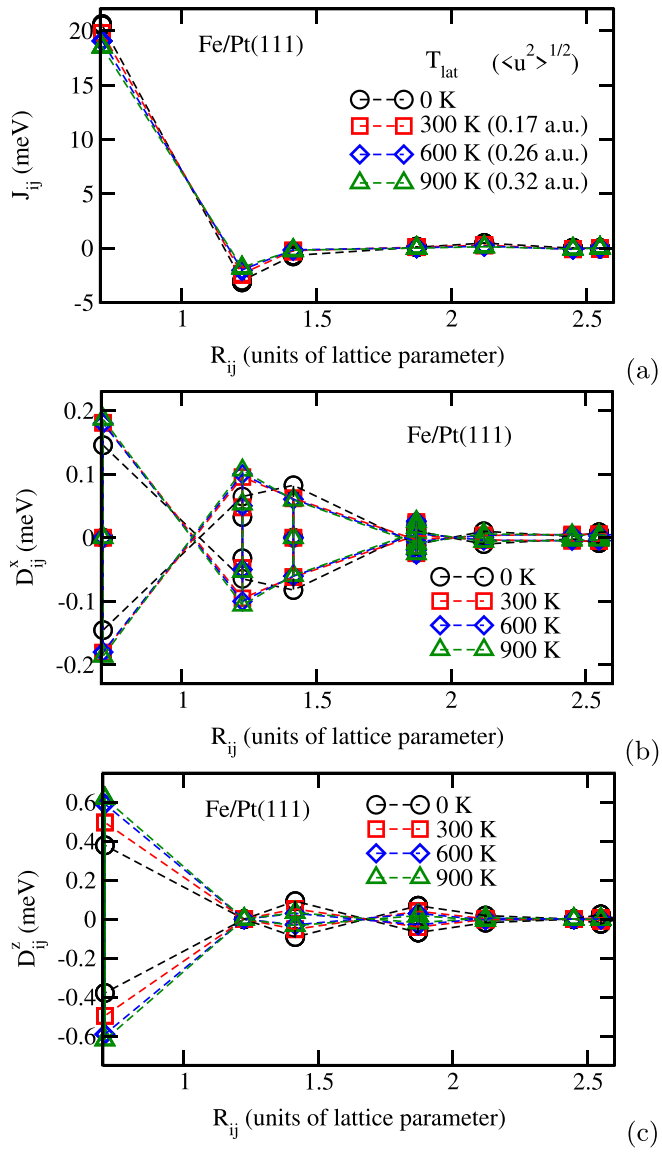

FIG. 10. Isotropic exchange coupling parameter J_{ij} (a), the x-component D^x_{ij} (b), and the z-component D^z_{ij} (c) of the DMI for 1 ML Fe on the Pt(111) surface for several values of the rms atomic displacement $(\langle u^2 \rangle_T)^{1/2}$ (given in parentheses) corresponding to different *lattice temperatures* T_{lat}.

layer systems considered are quasi-three-dimensional, and the use of a 3D Debye model for these systems seems nevertheless to be reasonably well justified.

As the Curie temperatures evaluated within the MFA are ≈800 K for Fe/Pt(111) and ≈900 K for Fe/Au(111), the highest *lattice temperature* used in our calculations is 900 K. Figures 10 and 11 show results for the Fe-Fe isotropic exchange interaction (a), the x (b), and the z component (c) of the DMI, calculated for the FM reference state of these systems. As one can see, in both cases a similar behavior has been found for isotropic exchange interactions J_{ij} as a function of the Fe-Fe distance R_{ij} with a weak dependence on the lattice temperature. On the other hand, the dependence of the DMI components, D^{α}_{ij}, on thermal lattice vibrations is much more pronounced. Interestingly, an opposite trend of

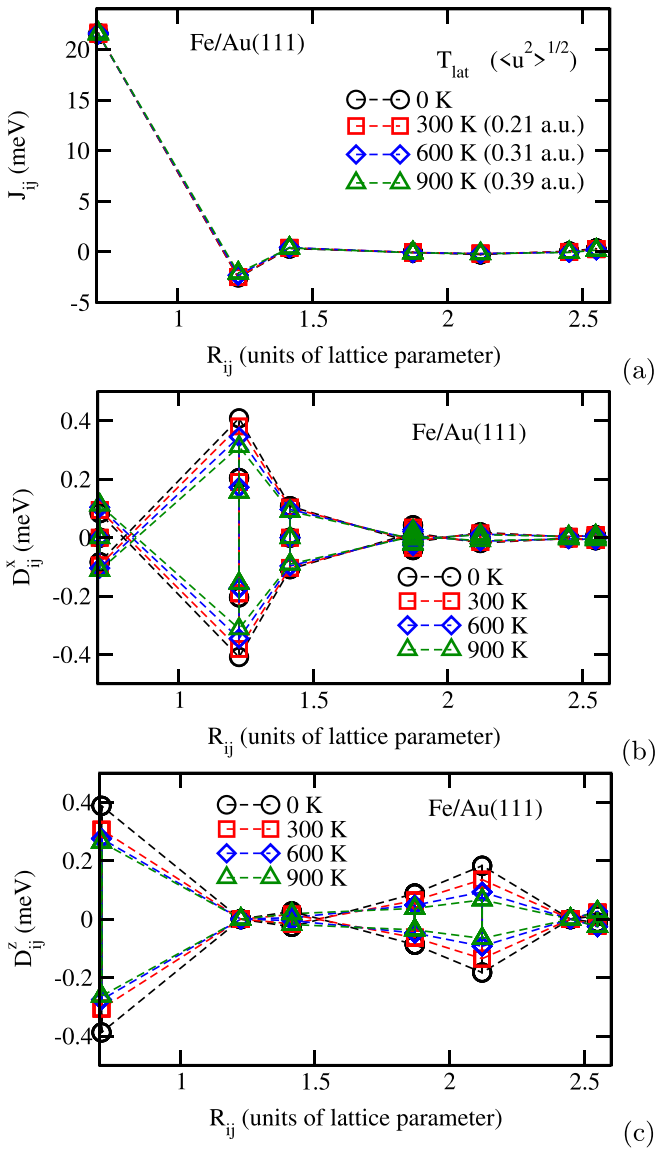

FIG. 11. Isotropic exchange coupling parameter J_{ij} (a), the x-component D^x_{ij} (b), and the z-component D^z_{ij} (c) of the DMI for 1 ML Fe/Au(111) for several values of the rms atomic displacement $(\langle u^2\rangle_T)^{1/2}$ (given in the parentheses) corresponding to different *lattice temperatures* T_{lat}.

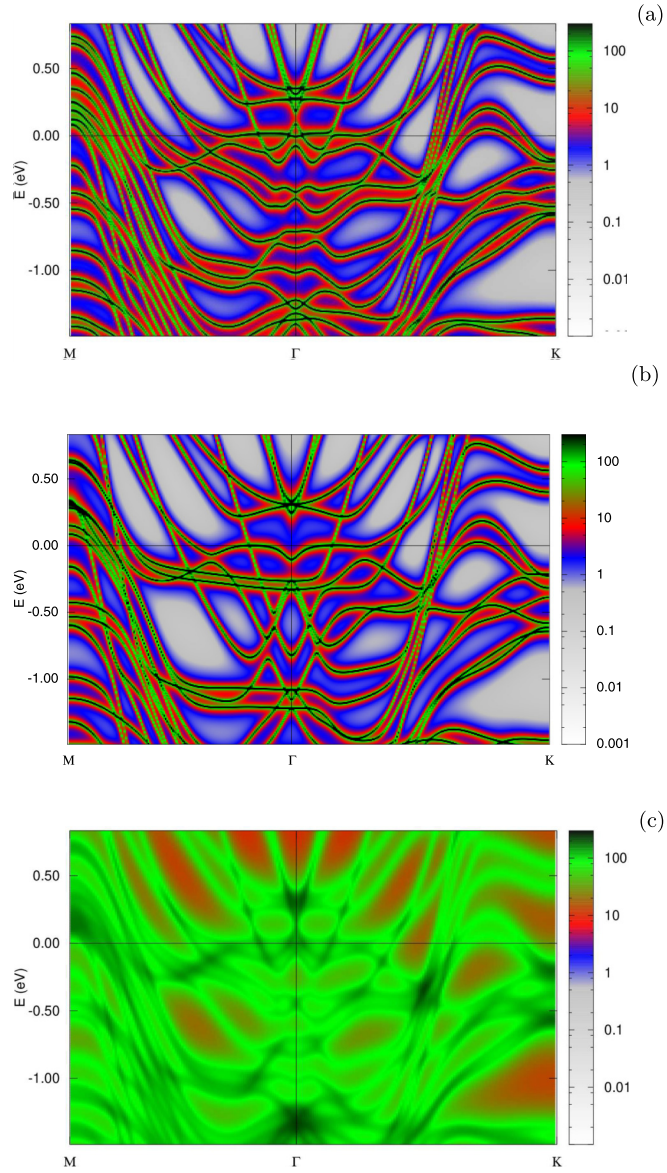

FIG. 12. Bloch spectral function calculated for 1 ML Fe/Pt(111) using two values of the imaginary part of the energy: 0.1 meV, with SOC (a) and without SOC (b), and 5 meV with SOC (c).

the temperature induced modifications of the D^{α}_{ij} parameters shows up for different Fe-Fe distances. A similar behavior can also be seen when comparing the first-neighbor DMI for the systems under consideration. While in the case of 1 ML Fe/Au(111) an increasing amplitude of thermal lattice vibrations results in a decrease of the Fe-Fe DMI [see Fig. 11(b)], the DMI increases with increasing *lattice temperature* in the case of 1 ML Fe/Pt(111). To get more insight concerning the influence of lattice vibrations on the exchange interactions, the nearest-neighbor exchange parameters have been calculated as a function of occupation for two different values of the lattice temperature. Figures 13 and 14 show the isotropic Fe-Fe exchange coupling parameter J_{01} (a) and z component of the DMI D^z_{01} (b). For the parameter J_{01} only a weak change caused by an increase of the *lattice temperature* can be seen over the whole regime of occupation numbers represented in the figures. In contrast to this, Figs. 13(b) and 14 show a very pronounced impact of the lattice vibrations on the parameter D^z_{01}. As one can see in the figures, D^z_{01} seen as a function of the occupation has a nonmonotonous behavior at low temperature with the observed "fine structure" associated with avoided crossings of the energy bands. These details of the electronic structure can be seen in Fig. 12(a) for 1 ML Fe/Pt(111) in the vicinity of the Fermi energy. The rapid changes of the DMI occur when the apparently varied Fermi level passes through an avoided crossing of the energy bands, which occurs due to spin-orbit coupling (SOC) (see discussion in Refs. [47,48]). The most prominent modifications of the band around the avoided crossing points occur in the vicinity of the Γ point both along the $\Gamma - M$ and $\Gamma - K$ directions, as well as in the middle of the $\Gamma - K$ direction of the Brillouin zone. This can

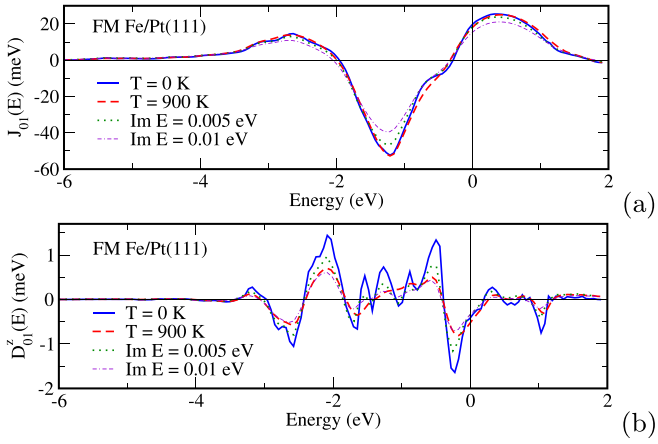

FIG. 13. Occupation dependent Fe-Fe exchange coupling parameter J_{01} (a) and z component of the DMI D^z_{01} in 1 ML Fe/Pt(111) calculated for two values of the *lattice temperature* T_{lat}. Dotted and dashed-dotted lines represent the results obtained with the imaginary energy part of 5 and 10 meV, respectively.

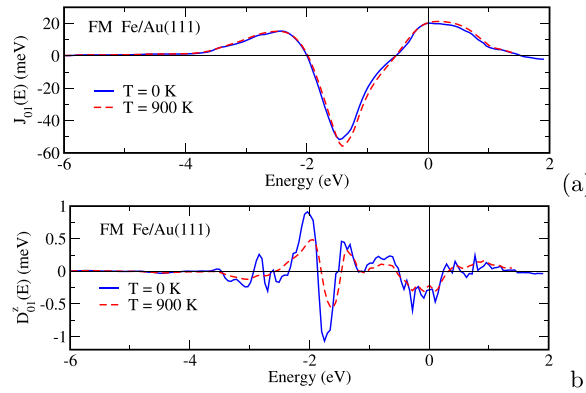

FIG. 14. Occupation dependent Fe-Fe exchange coupling parameter J_{01} (a) and z component of the DMI D^z_{01} in 1 ML Fe/Au(111) calculated for two values of the *lattice temperature* T_{lat}.

be easily seen by comparing the energy bands represented by the Bloch spectral functions in Figs. 12(a) and 12(b), which are calculated with (a) and without (b) SOC interaction taken into account. The prominent features in the DMI plots seen in Figs. 13(b) and 14(b) are created by those energy bands that give a dominant contribution to D^z_{01}. When the *lattice temperature* increases to $T_{\text{lat}} = 900$ K, the fine structure of $D^z_{01}(E)$ seen as a function of E is washed out for both systems. Partially, this can be attributed to a smearing of the energy bands due to an increasing electron scattering by the thermal lattice vibrations. This mechanism is demonstrated in Fig. 12(c) that represents the Bloch spectral function calculated for an imaginary part of the energy of 5 meV mimicking a decrease of the lifetime of the electronic states connected with the electron scattering by lattice vibrations. This modification of the electronic structure leads for 1 ML Fe/Pt(111) to the changes of $J_{01}(E)$ and $D^z_{01}(E)$ as functions of the energy shown in Figs. 13(a) and 13(b) by dotted lines. Dashed-dotted lines represent corresponding results obtained for an imaginary part of the energy of 10 meV. In the case of the DMI, one can see a decrease of the amplitude of modulations with energy when the imaginary part of the energy increases. However, comparing these results with the results obtained for $T_{\text{lat}} = 900$ K, it is obvious that the influence of thermal lattice vibrations on the exchange parameters also stems to a large extent from their impact on the matrix elements given in Eq. (3). Note also that, in contrast to the energy and orbital-specific smearing caused by the thermal lattice vibrations, the calculations using a fixed imaginary part for the energy give the same smearing for all energy bands.

V. SUMMARY

To summarize, the alloy analogy model was used to calculate the exchange coupling parameters taking into account randomly distributed atomic displacements in the lattice giving access this way to temperature induced modifications of the exchange parameters. Focusing both on the isotropic exchange and Dzyaloshinskii-Moriya interactions, it is demonstrated that—depending on the material—the effect of lattice vibrations on the exchange parameters can be rather significant and should be taken into account in simulations of finite-temperature magnetic properties of these systems. In particular, in the case of skyrmion hosting materials, thermal lattice vibrations, together with thermal spin fluctuations and lattice expansion, have an impact on the temperature dependent size as well as the stability of the skyrmion, as these are determined by the exchange interactions and magnetic anisotropy in the system.

Moreover, the present approach allows one to make a correction to the exchange coupling parameters in random alloys with alloy components having different atomic radius resulting in turn in randomly distributed atomic displacements. In fact, a significant impact of such static displacements on the residual electrical resistivity was demonstrated for high-entropy alloys [49].

ACKNOWLEDGMENT

Financial support by the DFG via SFB 1277 (Emergent Relativistic Effects in Condensed Matter—From Fundamental Aspects to Electronic Functionality) is gratefully acknowledged.

[1] H. Hasegawa and D. G. Pettifor, Phys. Rev. Lett. **50**, 130 (1983).
[2] F. Körmann, A. Dick, B. Grabowski, B. Hallstedt, T. Hickel, and J. Neugebauer, Phys. Rev. B **78**, 033102 (2008).
[3] F. Körmann, B. Grabowski, B. Dutta, T. Hickel, L. Mauger, B. Fultz, and J. Neugebauer, Phys. Rev. Lett. **113**, 165503 (2014).
[4] J. Fransson, D. Thonig, P. F. Bessarab, S. Bhattacharjee, J. Hellsvik, and L. Nordström, Phys. Rev. Materials **1**, 074404 (2017).
[5] J. Hellsvik, D. Thonig, K. Modin, D. Iuşan, A. Bergman, O. Eriksson, L. Bergqvist, and A. Delin, Phys. Rev. B **99**, 104302 (2019).

[6] T. C. Schulthess and W. H. Butler, J. Appl. Phys. **87**, 5759 (2000).
[7] B. Alling, A. V. Ruban, and I. A. Abrikosov, Phys. Rev. B **79**, 134417 (2009).
[8] H. Wang, P.-W. Ma, and C. H. Woo, Phys. Rev. B **82**, 144304 (2010).
[9] H. Ebert, S. Mankovsky, K. Chadova, S. Polesya, J. Minár, and D. Ködderitzsch, Phys. Rev. B **91**, 165132 (2015).
[10] W. H. Butler, Phys. Rev. B **31**, 3260 (1985).
[11] B. Velický, Phys. Rev. **184**, 614 (1969).
[12] H. Ebert, S. Mankovsky, D. Ködderitzsch, and P. J. Kelly, Phys. Rev. Lett. **107**, 066603 (2011).
[13] S. Mankovsky, D. Ködderitzsch, G. Woltersdorf, and H. Ebert, Phys. Rev. B **87**, 014430 (2013).
[14] B. L. Gyorffy, A. J. Pindor, J. Staunton, G. M. Stocks, and H. Winter, J. Phys. F: Met. Phys. **15**, 1337 (1985).
[15] B. L. Gyorffy, A. Barbieri, J. B. Staunton, W. A. Shelton, and G. M. Stocks, Physica B **172**, 35 (1991).
[16] J. B. Staunton and B. L. Gyorffy, Phys. Rev. Lett. **69**, 371 (1992).
[17] J. B. Staunton, S. Ostanin, S. S. A. Razee, B. L. Gyorffy, L. Szunyogh, B. Ginatempo, and E. Bruno, Phys. Rev. Lett. **93**, 257204 (2004).
[18] J. B. Staunton, L. Szunyogh, A. Buruzs, B. L. Gyorffy, S. Ostanin, and L. Udvardi, Phys. Rev. B **74**, 144411 (2006).
[19] A. Buruzs, P. Weinberger, L. Szunyogh, L. Udvardi, P. I. Chleboun, A. M. Fischer, and J. B. Staunton, Phys. Rev. B **76**, 064417 (2007).
[20] D. Böttcher, A. Ernst, and J. Henk, J. Magn. Magn. Mater. **324**, 610 (2012).
[21] L. Szunyogh and L. Udvardi, Philos. Mag. **78**, 617 (1998).
[22] R. F. Sabiryanov and S. S. Jaswal, Phys. Rev. Lett. **83**, 2062 (1999).
[23] S. Mankovsky, S. Polesya, H. Ebert, W. Bensch, O. Mathon, S. Pascarelli, and J. Minár, Phys. Rev. B **88**, 184108 (2013).
[24] B. Alling, F. Körmann, B. Grabowski, A. Glensk, I. A. Abrikosov, and J. Neugebauer, Phys. Rev. B **93**, 224411 (2016).
[25] E. Mozafari, B. Alling, M. P. Belov, and I. A. Abrikosov, Phys. Rev. B **97**, 035152 (2018).
[26] A. V. Ruban and O. E. Peil, Phys. Rev. B **97**, 174426 (2018).
[27] M. Di Gennaro, A. L. Miranda, T. A. Ostler, A. H. Romero, and M. J. Verstraete, Phys. Rev. B **97**, 214417 (2018).
[28] L. Udvardi, L. Szunyogh, K. Palotás, and P. Weinberger, Phys. Rev. B **68**, 104436 (2003).
[29] H. Ebert and S. Mankovsky, Phys. Rev. B **79**, 045209 (2009).
[30] M. E. Rose, *Relativistic Electron Theory* (Wiley, New York, 1961).
[31] H. Ebert, J. Braun, D. Ködderitzsch, and S. Mankovsky, Phys. Rev. B **93**, 075145 (2016).
[32] M. Shimizu and T. Kato, Phys. Lett. A **27**, 166 (1968).
[33] H. Böttger, *Principles of the Theory of Lattice Dynamics* (Akademie-Verlag, Berlin, 1983).
[34] J. o. Sólyom, *Fundamentals of the Physics of Solids* (Springer-Verlag, Berlin, Heidelberg, 2007).
[35] H. Ebert, D. Ködderitzsch, and J. Minár, Rep. Prog. Phys. **74**, 096501 (2011).
[36] H. Ebert *et al.*, The Munich SPR-KKR package, version 7.7, https://www.ebert.cup.uni-muenchen.de/en/software-en/13-sprkkr.
[37] S. H. Vosko, L. Wilk, and M. Nusair, Can. J. Phys. **58**, 1200 (1980).
[38] A. Buruzs, L. Szunyogh, and P. Weinberger, Philos. Mag. **88**, 2615 (2008).
[39] N. Ridley and H. Stuart, J. Phys. D: Appl. Phys. **1**, 1291 (1968).
[40] Y. O. Kvashnin, R. Cardias, A. Szilva, I. Di Marco, M. I. Katsnelson, A. I. Lichtenstein, L. Nordström, A. B. Klautau, and O. Eriksson, Phys. Rev. Lett. **116**, 217202 (2016).
[41] A. V. Ruban, S. Khmelevskyi, P. Mohn, and B. Johansson, Phys. Rev. B **75**, 054402 (2007).
[42] E. A. Owen and E. L. Yates, London, Edinburgh, Dublin Philos. Mag. J. Sci. **21**, 809 (1936).
[43] S. Polesya, S. Mankovsky, D. Ködderitzsch, J. Minár, and H. Ebert, Phys. Rev. B **93**, 024423 (2016).
[44] S. Schlotter, P. Agrawal, and G. S. D. Beach, Appl. Phys. Lett. **113**, 092402 (2018).
[45] Y. Zhou, R. Mansell, S. Valencia, F. Kronast, and S. van Dijken, Phys. Rev. B **101**, 054433 (2020).
[46] L. Nicolai and J. Minár, XPS limit in soft X-ray photoemission spectroscopy of Ag(001), in *Applied Physics of Condensed Matter (APCOM 2018)*, edited by J. Sitek, J. Vaida, and Igor Jamnicky, AIP Conf. Proc. No. 1996 (AIP, Melville, NY, 2018), p. 020033.
[47] T. Koretsune, N. Nagaosa, and R. Arita, Sci. Rep. **5**, 13302 (2015).
[48] L. M. Sandratskii, Phys. Rev. B **96**, 024450 (2017).
[49] S. Mu, G. D. Samolyuk, S. Wimmer, M. C. Troparevsky, S. N. Khan, S. Mankovsky, H. Ebert, and G. M. Stocks, npj Comput. Mater. **5**, 1 (2019).